LoRadar: An Efficient LoRa Channel Occupancy Acquirer based on Cross-channel Scanning

Fu Yu, Xiaolong Zheng, Liang Liu, Huadong Ma
Beijing University of Posts and Telecommunications, Beijing, P. R. China
{yufu, zhengxiaolong, liangliu, mhd}@bupt.edu.cn

***Abstract*—LoRa is widely deployed for various applications. Though the knowledge of the channel occupancy is the prerequisite of all aspects of network management, acquiring the channel occupancy for LoRa is challenging due to the large number of channels to be detected. In this paper, we propose LoRadar, a novel LoRa channel occupancy acquirer based on cross-channel scanning. Our in-depth study finds that Channel Activity Detection (CAD) in a narrow band can indicate the channel activities of wide bands because they have the same slope in the time-frequency domain. Based on our finding, we design the cross-channel scanning mechanism that infers the channel occupancy states of all the overlapping channels by the distribution of CAD results. We elaborately select and adjust the CAD settings to enhance the distribution features. We also design the pattern correction method to cope with distribution distortions. We implement LoRadar on commodity LoRa platforms and evaluate its performance on the indoor testbed and the outdoor deployed network. The experimental results show that LoRadar can achieve a detection accuracy of 0.99 and reduce the acquisition overhead by up to 0.90, compared to existing traversal-based methods.**

I. Introduction

As a low-power and long-range technique, LoRa has received extensive attention from industrial and academic circles [1]. It is widely used in various IoT applications such as localization service [2]–[5], environmental monitoring [6]–[12], and wireless sensing [13]–[15]. It provides flexible BW (Bandwidth) setting from 7.81KHz to 500KHz and SF (Spreading Factor) from 5 to 12 to satisfy the requirements of different scenarios. There are also many studies [16]–[20] focusing on improving the performance of LoRa networks. Nowadays, more than 130 operators globally provide large-scale LoRa service [21]. The explosive growth of LoRa devices significantly increases the development density and the channel occupancy ratio.

Facing such ever-expanding LoRa networks, it is crucial to monitor the channel occupancy to learn which channels are in use. On the one hand, acquiring channel occupancy is the prerequisite of network monitoring and management. We have to know which channels are in use before we can sniff the channel traffic or identify unauthorized illegal transmissions in a specific channel. Besides, when natural disasters occurring, quick channel occupancy detection can help rescuers search for surviving communication channels and even survivors. On the other hand, acquiring channel occupancy can help Medium Access Control (MAC) designs to select desired channels. For example, LMAC [22] relies on the channel occupancy information to allow a node access good channels by CSMA.

However, efficiently acquiring the LoRa channel occupancy is very challenging due to the large number of LoRa channels. Different from wireless technologies such as WiFi [23], ZigBee [24] that have strict standards of channel partition, LoRa supports diverse channel partitions and allows channels to overlap with each other. What's worse, in a physical channel, LoRa allows concurrent transmissions with different SF, which results in more logical channels. Hence, a LoRa channel is actually defined by the central frequency with specific BW and SF of the Chirp Spread Spectrum (CSS) modulation. Then the total number of LoRa channels is enormous. For a 500KHz frequency band, LoRa allows 7 physical channels, including four 125KHz, two 250KHz, and one 500KHz channels. For each physical channel, LoRa can use SF from 5 to 12 to obtain 8 logic channels. Then we have 56 channels just in a 500KHz frequency band. Taking the whole 915MHz ISM band of LoRa (902.3MHz-914.9MHz) into consideration, we will have up to 1400 LoRa channels to be detected!

Such a large number of channels makes channel occupancy acquisition difficult. Recent LoRa transceivers [25] [26], provide LoRa CAD (Channel Activity Detection) to detect activities in a specific LoRa channel by calculating the cross-correlation of the received LoRa symbol and the base up-chirp. If the result is beyond the predefined threshold, `CadDetected` interrupt is set to indicate the channel is busy. But directly using CAD to traverse a large number of channels is infeasible. First, our measurement results in Section II show that traversing all the channels in a 500KHz band once can takes more than 15 seconds, which is time- and energy-consuming. Second, we surprisingly find that CAD, which is quite reliable in a single channel, is no longer reliable when used in traversal detection. By carefully analyzing the results, we find that CAD experiences lots of false positives, even though we use the recommended CAD setting that is supposed to avoid false positives. Our in-depth analysis reveals that LoRa chirps with different BW and SF but have same slope in the time-frequency domain result in a high cross-correlation value when performing CAD in the overlapping narrow band, leading to CAD false positives.

The fact that CAD in a narrow channel has false positives caused by the wider channels inspires us to design a cross-channel scanning method that uses CAD results in a narrow channel to infer the occupancy of overlapping wide channels.

Our further in-depth studies verify the feasibility of cross-channel scanning. We find that *there are significant differences in the distribution of CAD positives caused by different wide channels within the same time.* This is because the chirps with same slope in different channels must have different symbol duration and the number of symbols of different channels within the same detection period will be different. This key observation inspires us to leverage cross-channel scanning to reduce the number of detected channels.

However, to accomplish such an idea, we still face three key challenges. First, to get the distributions, we have to perform multiple CADs. But the appropriate number of CADs is hard to decide. Too few CADs cannot reliably obtain the distributions while too many CADs will increase the baseline overhead. Second, due to the asynchronization between CAD and the LoRa symbol, distributions of CAD positives can be distorted, resulting in accuracy degradation. How to cope with the distorted distributions is challenging. Third, noise and interference from environment can generate unexpected false positives that disturb the distributions. How to eliminate their influence is also challenging.

To solve these challenges, we propose LoRadar, a novel LoRa channel occupancy acquirer that can quickly learn the occupancy of a larger number of LoRa channels. Based on our insightful observations, we propose the cross-channel scanning mechanism that learns the occupancy of wider channels by CAD in the narrow channel. We first carefully model the distributions of CAD positives for different narrow-wide channel pairs to obtain the stable differentiation patterns. Then we select the appropriate number of CADs to achieve a good trade-off between accuracy and overhead. Second, we investigate the root cause of distribution overlapping and then design a pattern correction algorithm to correct the shifted distribution caused by false negatives. Third, we propose an adaptive algorithm that dynamically adjusts the CAD parameters to reduce unexpected CAD false positives caused by environment noise. Finally, to further reduce the overhead, we design a conditional speed-up strategy that leverages prior detection results to opportunistically adjust the number of CADs.

The contributions of this work are summarized as follows.

- We propose LoRadar, a novel LoRa channel occupancy acquirer based on cross-channel scanning. LoRadar can efficiently learn the channel occupancy matrix to facilitate a diversity of LoRa applications such as network monitoring and management and MAC designs.
- We find that distributions of CAD results in a narrow channel can indicate activities in wider channels. Based on this key insight, we design the cross-channel scanning mechanism and solve several technical challenges, including scanning setting selection and adaption, and detection errors caused by distribution distortions.
- We implement LoRadar on commodity LoRa devices and extensively evaluate its performance. The experimental results demonstrate that LoRadar can acquire the LoRa channel occupancy with 0.95 accuracy within 1.5 seconds. The detection overhead is reduced by up to 87.3% with 72.5% accuracy improvement, compared to the traversal-based method.

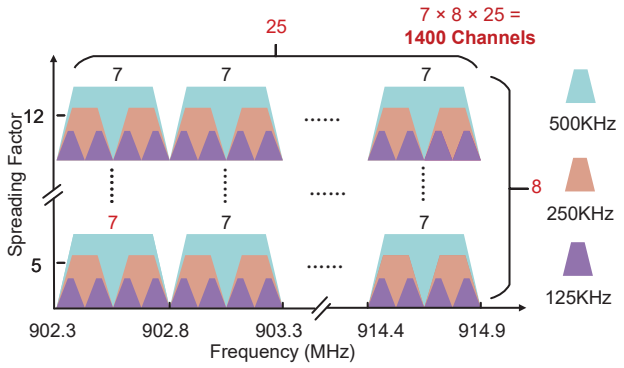

Fig. 1. LoRa channels to be detected in 915MHz ISM band.

The rest of this paper is organized as follows. We introduce the background and motivation of this work in Section II. Then we present the design of LoRadar in Section III and evaluation results in Section IV. We discuss the related work in Section V and finally conclude our work in Section VI.

II. Background & Motivation

The recent LoRa chips such as SX1262 [25] and SX1276 [26] introduce Channel Activity Detection (CAD) to detect LoRa symbols in a channel with given BW and SF. CAD calculates the cross-correlation between the received signal in one symbol duration T_{sym} and the template up-chirp signal. If the value is beyond the predefined threshold th, `CadDetected` interrupt will be triggered to indicate a busy channel. Two crucial CAD parameters, `CadDetPeak` and `CadSymbolNum`, can be configured to adapt to different environments. `CadDetPeak` is positively related to th. Increasing its value is beneficial to reduce false positives caused by noise. But a too high value will cause false negatives of weak signals. `CadSymbolNum` is the minimum number of continuous symbols that are detected before triggering `CadDetected` interrupt. A larger `CadSymbolNum` helps decrease false positives but brings longer execution time.

To acquire the channel occupancy by CAD, a naive way is to traverse all the channels and perform CAD in each channel. However, such a traversal-based method is too costly in terms of time and energy. Fig. 1 presents the channel plan in [27]. We have up to 1400 LoRa channels to be detected in 915MHz ISM band. Suppose we perform ten CADs in each channel, the total acquisition time with the suggested CAD setting can be up to 15 seconds for a single 500KHz band. Besides, we surprisingly find that CAD, which is reliable in a single channel, is no longer reliable when used in the traversal-based channel occupancy detection. The accuracy is far below the expectation because of the unexpected false positives.

After analyzing the pattern of false positives in depth, we find that CAD not only detects the existence of the LoRa chirp with given SF and BW but also responses to some

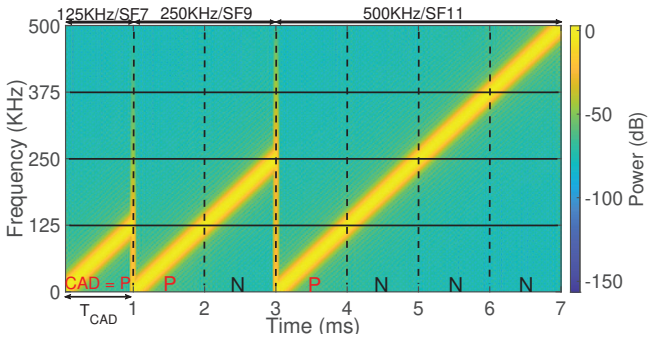

Fig. 2. LoRa chirps with different BW but same slope.

other special chirps. More specifically, chirps that have the same slope in time-frequency domain can also result in CAD positives. The reason behind this phenomenon is that CAD depends on cross-correlation computation to detect given LoRa chirps. As shown in Fig. 2, LoRa symbols with 125KHz/SF7, 250KHz/SF9 and 500KHz/SF11 have the same slope in the time-frequency domain. When performing CAD in the first 125KHz band, all of the three chirps can have a high cross-correlation value and therefore cause CAD positives. Since the slope of LoRa chirp depends on SF and BW, we identify that a group of LoRa chirps will have the same slope when satisfying the rule: BW doubles and SF increases by two.

Although false positives lower the detection accuracy, the observation reveals that the narrow-band CAD can indicate the channel occupancy of wider channels. We further investigate the results and find that though chirps with same slopes can all trigger CAD positives, the number of CAD positives within the same detection time is different for different chirps. From Fig. 2, we can clearly find that different chirps have different symbol duration and then have different number of occurrences in a narrow-band channel. Such a key insight inspires us to achieve cross-channel scanning that uses narrow-band CAD results to infer the occupancy of wider channels. By this way, the number of detected channels can be significantly reduced and the acquisition process can be accelerated.

Though attractive, implementing such an idea needs elaborate designs to address the CAD distribution distortions and obtain the desired distribution with minimum overhead.

III. Design

In this section, we first present an overview of LoRadar and then introduce the design details of each component.

A. Overview of LoRadar

Fig. 3 shows the framework of LoRadar that consists of four components. Given the channels to be detected, LoRadar first decides the suitable CAD scanning setting, including the number of CADs N_{CAD} in a detection window and CAD initial parameters. We analyze impacts of settings on both detection performance and overhead to decide the appropriate initial setting. During the online detection, LoRadar keeps estimating the environment noise and dynamically adjusts the

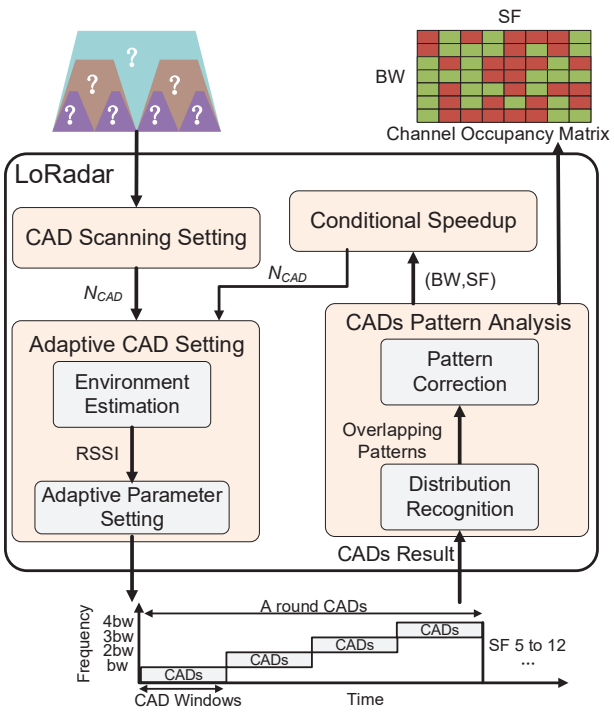

Fig. 3. Overview of LoRadar.

CAD setting accordingly. By eliminating false positives caused by noise, LoRadar can keep the noise from disturbing the desired distinguishable distributions. After deciding the CAD setting, LoRadar calls for the CAD operation provided by LoRa chips to obtain CAD results on each narrow channel. Then the results are analyzed by the CAD pattern analysis component. LoRadar decides which channels are occupied by comparing the number of CAD positives CAD_P with the valid range of CAD positives for each channel, including the narrow and wide channels. Due to distribution distortions caused by asynchronous probing and noise, LoRadar adopts a pattern correction component to check results with CAD_P equals to particular values where confusing distribution may occur. After correction, the final detection results on channel occupancy are used to update the channel occupancy matrix, which can be used by other applications such as MAC protocols, traffic sniffer, and network monitors. Besides, to reduce the detection overhead, LoRadar also designs a conditional speedup component to opportunistically adjust the CAD setting for next round according to the prior channel occupancy detection result.

B. CAD Scanning Setting

To achieve robust and efficient cross-channel scanning, the CAD scanning setting should be carefully designed, including CAD parameters and the number of CADs in a detection window. From the analysis in Section II, we have learn that we can use a CAD detection window with N_{CAD} continuous CADs to infer the occupancy states of different channels.

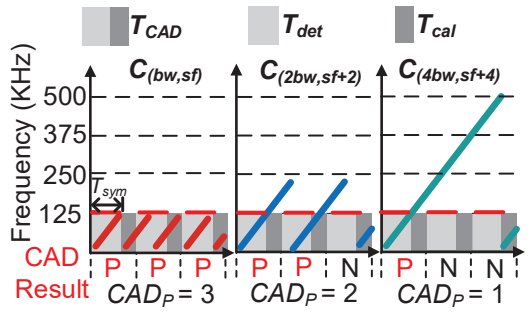

Fig. 4. Various CAD_P for LoRa symbols with same slope.

Fig. 4 presents an example of CAD results when three channels with the same slope in the time-frequency domain. The LoRa channel is denoted as $C_{(BW,SF)}$ to indicate a channel with bandwidth of BW and spreading factor of SF. We perform CAD with $N_{CAD} = 3$ in the first 125KHz channel. Each CAD duration T_{CAD} consists of the sampling time T_{det} and the computing time T_{cal}, which are described by the light and dark gray areas in Fig. 4. Due to the different symbol duration of these three channels, the number of symbols occur in one CAD detection window are different. Hence, the number of positive CAD results CAD_P will be 3, 2, and 1 for channel $C_{(bw,sf)}$, $C_{(2bw,sf+2)}$, and $C_{(4bw,sf+4)}$, respectively. Besides, CAD_P will be 0 when all channels are idle. Then, we can scan the four narrow channels to infer the channel occupancy of all overlapping channels. The example reveals that $N_{CAD} = 3$ is enough to differentiate the occurrence of different channels.

However, using only three CADs in a detection window cannot provide robust distribution patterns due to the small difference between different patterns. The unexpected CAD false positive or negative results can easily confuse the channel occupancy judgement. Hence, we increase N_{CAD} to enlarge the difference between distributions. But blindly using a large N_{CAD} significantly increases the baseline overhead in terms of both detection delay and energy consumption.

To determine the suitable CAD setting that can provide robust results with limited overhead, we first model the relationship between CAD_P and the number of occurred symbols of different channels with various N_{CAD}. Assuming CAD detection window is aligned with the symbol window, $N_{sym}^{(BW,SF)}$, the number of occurred symbols within the detection window for channel $C_{(BW,SF)}$, can be calculated by:

$$N_{sym}^{(BW,SF)} = [\frac{N_{CAD} \times T_{CAD} - T_{cal}}{T_{sym}^{BW,SF}}] \quad (1)$$

where $T_{sym}^{(BW,SF)}$ is the symbol duration for channel $C_{(BW,SF)}$ and $[\cdot]$ denotes the rounding operation. Since during the T_{cal} of final CAD, no signal is received and the final CAD result will not be influenced, we remove it from calculation. Suppose $T_{sym}^{(bw,sf)}$ is t, then $T_{sym}^{(2bw,sf+2)}$ and $T_{sym}^{(4bw,sf+4)}$ should be $2t$ and $4t$. For the commonly used BW of 125kHz, T_{CAD} is about $1.6t$ because T_{cal} is about $0.6t$ [28]. Using t to rewrite Eq. (1), we can obtain the following equations.

$$N_{sym}^{(BW,SF)} = [\frac{1.6 \times N_{CAD} - 0.6}{m}] \quad (2)$$

where $m = 1, 2, 4$ for (bw,sf), (2bw,sf+2), (4bw,sf+4). Then, we can calculate the $CAD_{valid}^{(BW,SF)}$ for different channels and measure the minimum difference among the overlapping channels with different N_{CAD} by:

$$CAD_{valid}^{(BW,SF)} = \min\{N_{sym}^{(BW,SF)}, N_{CAD}\} \quad (3)$$

The results are shown in Table I. We can observe a step growth of the minimum difference among channels with the increase of N_{CAD}. To obtain robustness, increasing N_{CAD} to 13 to obtain a minimum difference of 3 is too costly. Hence, in our current implementation, we select $N_{CAD} = 7$ to balance the robustness and time consumption.

The above calculation has an assumption that CAD detection window is aligned with LoRa chirps. But in practice, such an assumption rarely holds and more symbols can occur in a detection window. Namely, for a given channel $C_{(BW,SF)}$, the valid CAD_P can be $\{CAD_{valid}^{(BW,SF)}, CAD_{valid}^{(BW,SF)} + 1\}$. Given $N_{CAD} = 7$, the $CAD_{valid}^{(BW,SF)}$ are shown in Table II. Note that since CAD_P cannot exceed N_{CAD}, $CAD_{valid}^{(bw,sf)}$ is only 7. For the idle case, the asynchronization will not cause false positives, then its valid CAD_P is still 0.

Besides N_{CAD}, we also optimize the CAD parameter, `CadSymbolNum`. By default setting [28], `CadSymbolNum` is set to 2 to avoid false positives. However, we want to encourage helpful false positives to achieve cross-channel scanning. What's more, using `CadSymbolNum` of 2 means each CAD is over two symbols, which takes more time. Hence, we set `CadSymbolNum` to 1 in our design to achieve cross-channel scanning with less overhead.

To verify the effectiveness of our setting, we perform a validation experiment to study the detection error rate and

TABLE I

THE VALID $CAD_{valid}^{(BW,SF)}$ FOR DIFFERENT CHANNELS AND THE MINIMUM DIFFERENCE AMONG CHANNELS WITH DIFFERENT N_{CAD}.

N_{CAD} \ (BW,SF)	Idle	(4bw,sf+4)	(2bw,sf+2)	(bw,sf)	minimum difference
3	0	1	2	3	**1**
5	0	2	4	5	1
7	0	3	5	7	**2**
9	0	4	7	9	2
11	0	4	9	11	2
13	0	5	10	13	**3**
15	0	6	12	15	3

TABLE II

THE VALID $CAD_{valid}^{(BW,SF)}$ FOR CHANNEL $C_{(BW,SF)}$.

Channel $C_{(BW,SF)}$	Idle	(4bw,sf+4)	(2bw,sf+2)	(bw,sf)
$CAD_{valid}^{(BW,SF)}$	0	{3,4}	{5,6}	7

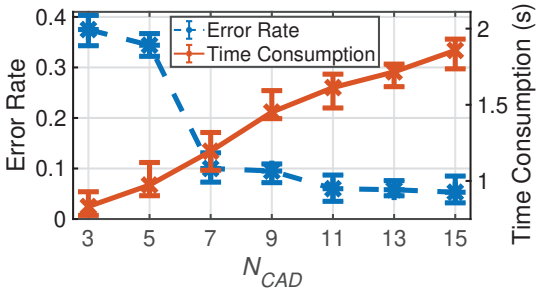

Fig. 5. Error rate and time cost when using different N_{CAD}.

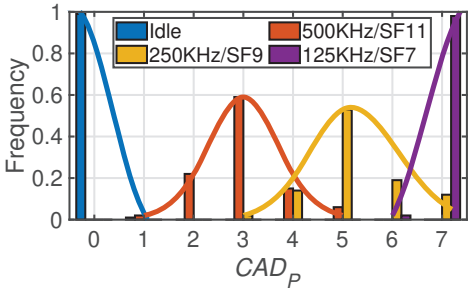

Fig. 6. The distribution of CAD_P when N_{CAD} is 7.

time cost when using different N_{CAD}. The results are shown in Fig. 5. We can find the time cost increases linearly with N_{CAD}, as expected. We can also find that $N_{CAD} = 7$ can dramatically reduce the error rate to 0.1. Further increasing N_{CAD} can only bring marginal improvement but have much larger time cost. The results verify our setting can provide a good balance between accuracy and time cost.

C. Adaptive CAD Setting

The results in Fig. 5 show that though LoRadar adopts a relaxed valid range of $CAD_{valid}^{(BW,SF)}$ to enhance the robustness, the detection error rate is still higher than expectation. We further analyze the CAD positive distributions to investigate the reason behind. Without losing generality, we take the results of channel $C_{(125KHz,SF7)}$, $C_{(250KHz,SF9)}$ and $C_{(500KHz,SF11)}$ as the example. For other channel groups, the results are similar. We plot the CAD positive distributions of these three channels in Fig. 6. We can clearly find four frequency peaks that correspond to idle and other three channels. But for all the channels, there exist cases where CAD_P is out of the valid range in Table II. The overlapping distributions result in confusion of channel occupancy and lead to detection errors.

The overlapping distribution problem for a channel can be divided into two cases, the left shifted overlapping occurs when $CAD_P < CAD_{valid}^{(BW,SF)}$ and the right shifted overlapping occurs when $CAD_P > CAD_{valid}^{(BW,SF)} + 1$. The reason behind the left shift is that LoRa chirps can happen in T_{cal} and then the node fails to capture chirp activities, leading to CAD false negatives. To cope with the left shift, we propose a pattern correction algorithm in the CAD pattern analysis component that will be introduced in Section III-D. On the other hand, the right shift is the result of false positives caused by the unexpected interference from the ambient environment.

In background section, we have discussed that the CAD parameter `CadDetPeak` can suppress false positives. The default setting of `CadDetPeak` is recommended based on the environment with noise strength of -115dBm [28]. But in practice, the coexisting interference strength can be larger than that, leading to false positives. However, using a too high `CadDetPeak` will cause false negatives for the weak signals, which is unwanted to both communication and occupancy detection. How to dynamically adjust its value is non-trivial.

TABLE III
THE FALSE POSITIVE RATE OF CAD WITH DIFFERENT CADDETPEAK UNDER DIFFERENT NOISE INTENSITIES.

Noise (dBm) \ CadDetPeak	22	25	28	31
$[-75,-55)$	0.17	0.11	0.09	**0.00**
$[-95,-75)$	0.14	0.13	**0.01**	0.01
$[-115,-95)$	0.08	**0.01**	0.00	0.00

To solve this problem, we propose an RSSI-based adaptive CAD setting algorithm. Based on our measurements in various environments, we find that RSSI can reflect the interference intensity and then guide the selection of `CadDetPeak`. The measurement results are shown in Table III. We can find that to obtain a false positive rate lower than 0.01, `CadDetPeak` should be set differently for different noise intensities. But for every 20dBm increase of the interference strength, increasing `CadDetPeak` by 3 is good enough.

Based on this observation, we propose the RSSI-based CAD parameter adaption method. We first obtain the average RSSI value $RSSI_{ave}$ to learn the noise intensity in channel before performing CAD. The RSSI for recommended setting is denoted as $RSSI_{min} = -115dBm$. Then we can calibrate the value of `CadDetPeak` by adding an offset, δ, which can be calculated as follows.

$$\delta = k \times R_{step} \tag{4}$$

where R_{step} is set to 3 according to our empirical experience, and k is:

$$k = \lfloor \frac{RSSI_{ave} - RSSI_{min}}{20} \rfloor + 1 \tag{5}$$

Then we add δ to the recommended setting in [28] when performing CAD. Note that a node only takes about $2ms$ to get $RSSI_{ave}$ in a CAD window, which incurs negligible overhead.

Another adaptive CAD setting is the number of CADs executed in each channel. To reduce the energy consumption, a node will first periodically perform CAD, each of h times. The period is set according to the expected channel activity occurrence probability and h is smaller than N_{CAD}. When CAD reports positive during the periodical h executions, LoRadar starts executing CAD N_{CAD} times continuously to obtain the

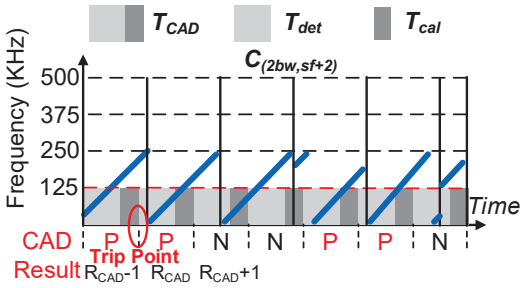

Fig. 7. LoRa symbol of (2bw,sf+2) with trip point.

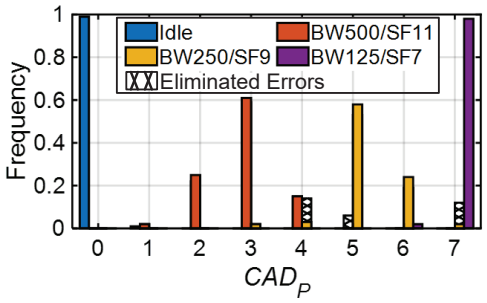

Fig. 8. The distribution of CAD_P with $N_{CAD} = 7$ after pattern correction.

distribution patterns. If no positive reports during h times CAD, the channel is regarded as idle.

D. Pattern Analysis

After performing CAD in the channel, we can obtain the CAD result, S_{CAD}, a sequence of seven CAD results, in which 0 and 1 represent negative and positive respectively. The pattern analysis component first classifies the CAD_P according to the $CAD_{valid}^{(BW,SF)}$ in Table II. Due to our adaptive CAD setting mechanism, we solve the right shift problem. Hence, we only consider the left shift problem here, namely, the false negatives due to the asynchronization between CAD detection window and symbol window.

By analyzing the results in Fig. 6 and Table II, we can learn that the left shift problem will cause confusions at CAD_P =2, 4, and 6 due to the distribution shift of channel $C_{(4bw,sf+4)}$, $C_{(2bw,sf+2)}$, and $C_{(bw,sf)}$. For $CAD_P = 2$, we can simply regard it as channel $C_{(4bw,sf+4)}$ because there is no other valid channel in this range. For $CAD_P = 6$, it can be recognized as $C_{(2bw,sf+2)}$ because the probability that $C_{(bw,sf)}$ shifts to 6 is small due to the low probability that one whole short symbol completely falls out of the CAD detection period. The results in Fig. 6 shows that the false negatives of the left shift for $C_{(bw,sf)}$ is only 0.02. For $CAD_P = 4$, it has a high occurrence frequency and brings serious accuracy degradation. As a result, we have to differentiate they are the valid results of the wider channel $C_{(4bw,sf+4)}$ or the left-shifted results of the narrower channel $C_{(2bw,sf+2)}$.

According to above analysis, we can further extend the valid $CAD_{valid}^{(BW,SF)}$ for different channels in Table IV. Specially, when $CAD_P = 4$, the results will be further corrected by our pattern correction method. Another special case is $CAD_P = 1$. Since the probability that $C_{(4bw,sf+4)}$ shifts to $CAD_P = 1$ is low, we simply regards $CAD_P = 1$ as idle.

We propose a trip-point based CAD pattern correction method to solve the confusing left shift problem. The trip point is defined as the symbol boundary between chirps during two continuous CAD positives. Since a trip point happens at the boundary of two chirps, it can indicate the start of a symbol. Then we can infer the active channel by the location of the next CAD positive, because the different periods of a symbol for different channel will lead to different locations of the next positive. For example, in Fig. 7, the trip point that happens at

TABLE IV
THE ROBUST VALID RANGE $CAD_{valid}^{(BW,SF)}$ FOR CHANNEL $C_{(BW,SF)}$.

Channel (BW,SF)	Idle	(4bw,sf+4)	(2bw,sf+2)	(bw,sf)
$CAD_{valid}^{(BW,SF)}$	{0,1}	{2,3,4}	{5,6}	7

the first and second CADs indicates that there is a symbol starting in the second CAD, which is denoted as $R_{CAD} = 2$. Hence, if $CAD_{R_{CAD}+3}$ and $CAD_{R_{CAD}+4}$ are both positive, then it must be $C_{(2bw,sf+2)}$ in use because they are the multiple of the symbol period of $C_{(2bw,sf+2)}$. Based on above condition, our pattern correction algorithm tests the hypothesis that $CAD_P = 4$ is caused by $C_{(2bw,sf+2)}$. If the hypothesis doesn't hold, we regard $CAD_P = 4$ is the valid result of $C_{(4bw,sf+4)}$. For the example in Fig. 7, we can find that the fifth and sixth CADs are both positive, then the hypothesis holds. We can correct the identification result from $C_{(4bw,sf+4)}$ to $C_{(2bw,sf+2)}$.

By pattern analysis, we can effectively remove false positives by parameter adaption and correct false negatives by pattern correction. We plot the distribution of CAD_P after correction and parameter adaptation in Fig. 8. The eliminated errors are highlighted by the grid shadow. We can find that the frequency of each overlapping distribution is lower than 0.03. The results can demonstrate the robustness of our cross-channel scanning design.

For the crowded spectrum that different channels occur in the same detection window in a narrow channel, we can leverage the detection results from neighboring channel to judge the state of the wide channel they shared.

E. Conditional Speedup

To further reduce the time delay, we leverage the previous detection result to opportunistically reduce N_{CAD}. For narrow channels covered by a wider channel, if one of them has already identified the state of the wide channel, then N_{CAD} can be reduced because we only need to judge the state of the narrow channel. Fig. 9 shows an example of conditional speedup. When the CAD results in the narrow channel $CH2$ are all negatives, indicating the idle state of two wider channels. Then we can reduce N_{CAD} for the neighboring narrow channel $CH1$ because we only need a small number of CADs to judge the state of the neighboring channel .

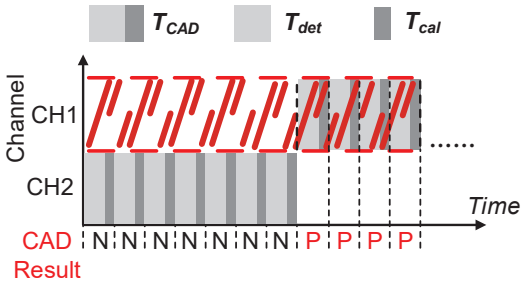

Fig. 9. Conditional speedup.

Our conditional speedup method works as follows. When wide channels are idle, we can safely reduce N_{CAD} to $\lceil \frac{N_{CAD}}{2} \rceil$ for the following narrow channels because there is no wider channel causes confusing false positives. But when the wide channels are busy, we adopt a conservative speedup principle. We only reduce N_{CAD} to $\lceil \frac{N_{CAD}}{2} \rceil$ when the much wider channel $C_{(4bw,sf+4)}$ is detected but keep N_{CAD} unchanged when the channel $C_{(2bw,sf+2)}$ is detected as busy. This is because the activities in channel $C_{(2bw,sf+2)}$ can cause false positives and disturb the distributions if reducing N_{CAD}.

IV. Evaluation

A. Experiment Setting

We implement LoRadar on commodity LoRa platforms with STML073RZ MCU and SX1262 LoRa transceiver. To evaluate the performance of LoRadar, we build an indoor testbed and deploy a real-word outdoor LoRa network.

The indoor testbed consists of 20 nodes, as shown in Fig. 10(a). One of the nodes acts as the channel occupancy acquirer and the other nodes are LoRa users, each of which runs in a selected channel in the 900MHz frequency band. Fig. 10(b) shows the outdoor deployment of a fifteen-node LoRa network in a $63,206m^2$ campus area, where 3 nodes are deployed in each location. We control the distance and transmission power to obtain LoRa links with different SNR. When evaluating under high channel occupancy ratios, we let each node performs channel hopping to emulate the occupancy of multiple channels.

For comparison, we implement two methods as baseline. The first one is the naive traversal used in existing methods [22]. We also implement an improved traversal method by using a two-step detection that can reduce the time cost. For each traversed channel, the adaptive traversal method will first perform a small number of CADs with our efficient setting and only execute N_{CAD} CADs with the default setting when the first phase reports a positive CAD. By this way, the adaptive traversal method will reduce time cost when channel is idle.

We alternately execute the three methods on one node to compare the performances of them. Without losing generality, our experiments focus on the performance when detecting 56 LoRa channels in a 500KHz frequency band. For more wider frequency band, LoRa has to divide them into physical channels with bandwidth up to 500KHz. As a result, the performance of multiple 500KHz bands can be simply the multiple of single 500KHz band.

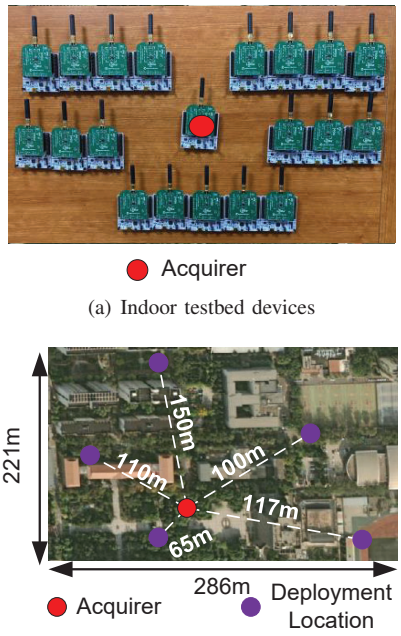

(a) Indoor testbed devices

(b) Outdoor deployment

Fig. 10. Indoor and outdoor LoRa networks

B. Performance of LoRadar under Different Conditions

The design goal of LoRadar is efficiently and accurately acquiring LoRa channel occupancy. We first evaluate the performance of LoRadar in different conditions. We conduct the experiments on our indoor testbed and compare LoRadar with the baselines.

1) Different Ratio of Occupied Channels: We first investigate the performance under different ratio of occupied channels. We vary the ratio of occupied channels from 0 (idle) to 0.7. Fig. 11 shows the time consumption and detection accuracy. From Fig. 11(a), we can find that with the increase of the ratio of occupied channels, naive traversal keeps a high time consumption, $11.0s$. The adaptive traversal has a low time consumption when the ratio is low because of our two-step CAD improvement. But when the ratio increase, the false positives caused by other channels will significantly increase the number of CADs executed. Then adaptive traversal has an obviously increased time consumption, which can be $8.4s$ when the ratio is 0.7. Thanks to the cross-channel scanning, the time consumption of LoRadar only increases from $1.0s$ to $2.1s$, when the ratio increases from 0 to 0.7. LoRadar can reduce the time consumption by up to 90.1% and 74.6%, compared to the naive and adaptive traversal methods respectively.

Though fast, LoRadar achieves the highest accuracy among all the methods. The accuracy of LoRadar only decreases from 0.99 to 0.91 when the ratio increases from 0 to 0.7. But for the traversal-based method, the accuracy can be lower than 0.6. This is because LoRadar can distinguish the positives

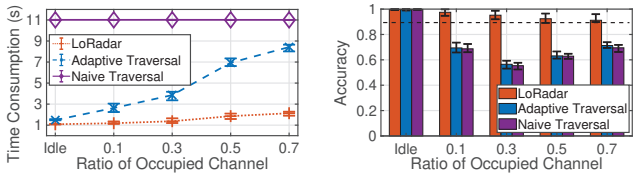

(a) Time consumption (b) Accuracy

Fig. 11. Performance under different ratio of occupied channels.

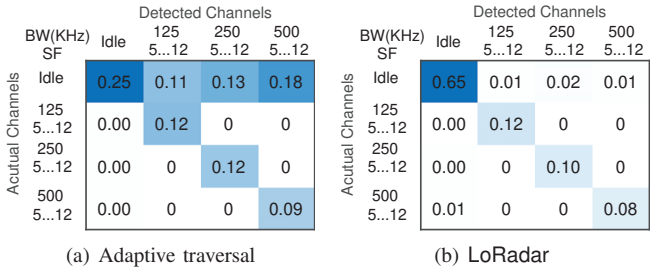

(a) Adaptive traversal (b) LoRadar

Fig. 12. Confusion matrix when the ratio of occupied channels is 0.3.

caused by different channels with the same chirp slope. But the traversal-based methods will judge the current channel as busy as long as CADs are positive, which causes serious false positives when the ratio of occupied channels is high. In Fig. 12, we present the confusion matrix of LoRadar and adaptive traversal when the ratio of occupied channel is 0.3. We omit the results of naive traversal because it is similar to the adaptive method. We can clearly observe a much higher false positive rate because the activities in wider channel cause CAD positives of the idle narrow channels.

2) Different SNR: We then study the performance of LoRadar under different SNR. Fig. 13 presents the results when we vary the median of SNR from -13dB to 11dB. The ratio of occupied channels is set to 0.3. From Fig. 13(a), we can find that LoRadar maintain a stable time consumption, which is 1.4s on average. Fig. 13(b) shows that LoRadar can achieve the high accuracy for all the SNR settings. The average accuracy is 0.95. This is because the cross-correlation of CAD doesn't depend on SNR and can detect signal with a low SNR. The other two baseline methods also have stable performance because they are also based on CAD. But due to the time-consuming traversal, the average time consumption of naive traversal and adaptive traversal is 10.9s and 3.8s, which are 7.8× and 2.7× larger than the time consumption of LoRadar. And due to inability of recognizing false positives, naive and adaptive traversal methods achieve the accuracy of 0.57 and 0.58, which are 40% and 39% lower than LoRadar's accuracy.

3) Different Noise Intensity: We also study the performance under various noise intensity. The results are shown in Fig. 14. We observe similar results to Fig. 13. The average time consumption of naive traversal, adaptive traversal, and LoRadar are 11.0s, 3.8s, and 1.4s respectively. LoRadar still achieves the highest accuracy, which is 0.94. The naive and adaptive traversal methods can only achieve the accuracy of

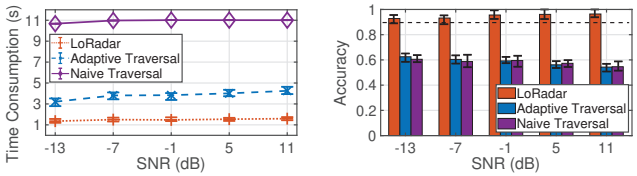

(a) Time consumption (b) Accuracy

Fig. 13. Performance under different SNR.

0.57 and 0.56 on average. The stable accuracy of LoRadar demonstrates that our adaptive CAD settings can effectively avoid the false positives caused by varying noise intensities. Two baseline methods also achieve the stable accuracy because they use the recommended CAD setting with a high `CadSymbolNum`. Though they can resist the varying noise, their setting is time-consuming.

C. Performance of LoRadar's Components

1) Pattern Correction: To study the performance of pattern correction algorithm, we compare the performance of LoRadar with and without pattern correction. Fig .15 shows the accuracy results when varying the ratio of occupied channels. For LoRadar without pattern correction, the accuracy significantly decreases from 0.99 to 0.81 when varying the ratio from 0 to 0.7. The more channels are occupied, the higher probability of overlapping distributions is. Hence, the performance degrades. But with the help of pattern correction, LoRadar can keeps an accuracy of 0.91, which is 12.3% higher than LoRadar without pattern correction. The results validate the efficiency of our pattern correction algorithm.

2) Conditional Speedup: The conditional speedup module aims to reduce the time consumption by leveraging the previous detected results. We compare the performance of LoRadar with and without conditional speedup in Fig. 16. From Fig .16(a), we can find that conditional speedup can reduce the time consumption by up to 0.29s. On average, the time consumption of LoRadar with conditional speedup is 8.6% lower than the time consumption of LoRadar without conditional speedup. Meanwhile, from Fig .16(b), we can find that conditional speedup doesn't degrade the accuracy.

D. Outdoor Deployment

We also evaluate LoRadar in an outdoor environment. 15 nodes are deployed at five locations in a campus, as shown in Fig. 10(b). We emulate different ratio of occupied channels by turning on different number of nodes and enabling channel hopping. The results are shown in Fig. 17. Fig. 17(a) shows that LoRadar achieves the highest accuracy among the three methods. The average accuracy of LoRadar is 0.94, which is 26.2% and 26.9% higher than the naive and adaptive traversal methods on average. From Fig. 17(b), we can find that LoRadar can reduce the time consumption of the naive and adaptive traversal methods by 50.7% and 85.6% on average. The results are similar to the results on the indoor testbed.

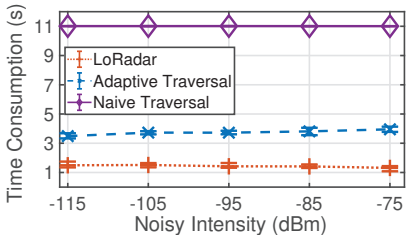

(a) Time consumption

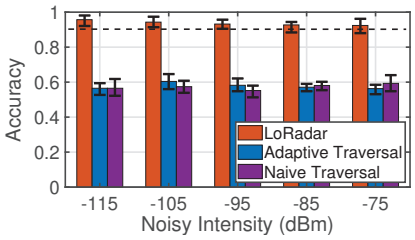

(b) Accuracy

Fig. 14. Performance under different noise intensity.

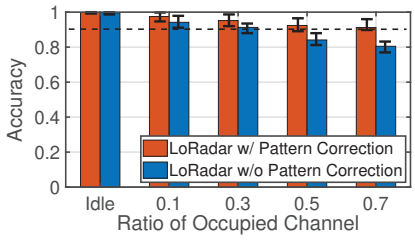

Fig. 15. Accuracy of LoRadar with and without pattern correction.

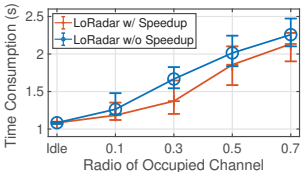

(a) Time consumption

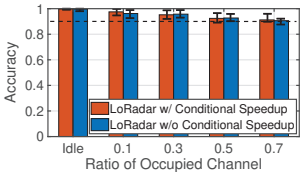

(b) Accuracy

Fig. 16. Performance of LoRadar with and without conditional speedup.

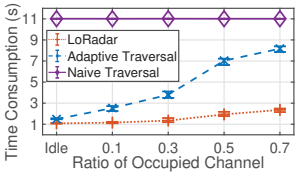

(a) Time consumption

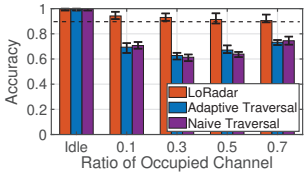

(b) Accuracy

Fig. 17. Performance in outdoor deployment.

The results show that LoRadar can effectively acquire LoRa channel occupancy in both indoor and outdoor environments.

V. Related Work

According to the detection object, channel occupancy detection can be divided into: single channel occupancy detection that learns the activities in a specific channel, and multiple channel occupancy detection that learns which channels are in use for the whole spectrum.

For single channel detection, RSSI is widely used in WiFi and Zigbee. However, RSSI based methods do not work for LoRa because the LoRa CSS signal can be below the noisy floor. Besides, LoRa supports the multiplexing of a physical channel by different SF. Semtech provides CAD in recent LoRa chips to detect the LoRa activity in a channel. Existing studies [22], [29]–[33] have verified that CAD can effectively detect the channel occupancy in a single channel. DeepSense [34] proposes a deep learning based method to achieve carrier sensing from the spectrogram of a channel. Existing studies about concurrent decoding [35]–[39] detect LoRa traffic by preamble detection.

For multiple channel detection, LMAC [22] combines the naive traversal-based CAD detection and information from the gateway to build the global channel occupancy matrix. But the traversal-based method is inefficient. The LoRa sniffer is designed in [40], [41]. They leverage the multi-channel reception ability of LoRa gateway chips or software-defined radio to monitor the LoRa packets. Besides the hardware restriction, they cannot detect the activities of channels with different BW at the same time. Our study focuses on multiple channel occupancy detection. Different from existing method, we propose the cross-channel scanning based on our new finding that CAD in narrow band can indicate the activities of channels with wider bands. Hence, we achieve an efficient LoRa channel occupancy acquirer.

VI. Conclusion

In this paper, we propose LoRadar, a cross-channel scanning based LoRa channel occupancy acquirer that can quickly learn the occupancy state for a large number of LoRa channels. Our in-depth study finds that CAD on a narrow band can indicate the occupancy states of overlapping channels with wider bands. Based on this key insight, we propose the cross-channel scanning method that can distinguish the channels based on the distributions of CAD results on a narrow band. We elaborately select the CAD setting and propose a RSSI-based CAD adaptation method to obtain the credible distribution. We propose the pattern correction algorithm to enhance the detection accuracy. We also design a conditional speedup mechanism to further reduce the detection overhead. The experimental results show that LoRadar can achieve the detection accuracy of 0.99 and reduce the time consumption by up to 0.90, compared to existing traversal-based methods. The authors have provided public access to their code at https://github.com/yufu186/LoRadar-INFOCOM-2022.

Acknowledgment

This work is supported in part by the National Natural Science Foundation of China under Grant 62072050 and Grant 61932013, the A3 Foresight Program of NSFC under Grant 62061146002, the Funds for Creative Research Groups of China under Grant 61921003, and the Funds for International Cooperation and Exchange of NSFC under Grant 61720106007. Xiaolong Zheng is the corresponding author.

REFERENCES

[1] C. LI and Z. CAO, "Lora networking techniques for large-scale and long-term iot: A down-to-top survey," *ACM Computing Surveys (CSUR)*, 2022.

[2] Y. Lin, W. Dong, Y. Gao, and T. Gu, "Sateloc: A virtual fingerprinting approach to outdoor lora localization using satellite images," *ACM Transactions on Sensor Networks*, vol. 17, no. 4, pp. 1–28, 2021.

[3] A. Bansal, A. Gadre, V. Singh, A. Rowe, B. Iannucci, and S. Kumar, "Owll: Accurate lora localization using the tv whitespaces," in *Proceedings of IEEE IPSN*, 2021.

[4] A. Mackey and P. Spachos, "Lora-based localization system for emergency services in gps-less environments," in *Proceedings of IEEE INFOCOM WKSHPS*, 2019.

[5] A. Olesiński and Z. Piotrowski, "An adaptive energy saving algorithm for an rssi-based localization system in mobile radio sensors," *Sensors*, vol. 21, no. 12, pp. 3987–3999, 2021.

[6] W. Du, Z. Xing, M. Li, B. He, L. H. C. Chua, and H. Miao, "Optimal sensor placement and measurement of wind for water quality studies in urban reservoirs," in *Proceedings of IEEE ICNP*, 2014.

[7] Y. Wang, X. Zheng, L. Liu, and H. Ma, "Polartracker: Attitude-aware channel access for floating low power wide area networks," in *Proceedings of IEEE INFOCOM*, 2021.

[8] B. Ngom, M. Diallo, B. Gueye, and N. Marilleau, "Lora-based measurement station for water quality monitoring: Case of botanical garden pool," in *Proceedings of IEEE SAS*, 2019.

[9] J. Botero-valencia, L. Castano-Londono, D. Marquez-Viloria, and M. Rico-Garcia, "Data reduction in a low-cost environmental monitoring system based on lora for wsn," *IEEE Internet of Things Journal*, vol. 6, no. 2, pp. 3024–3030, 2019.

[10] H.-C. Lee and K.-H. Ke, "Monitoring of large-area iot sensors using a lora wireless mesh network system: Design and evaluation," *IEEE Transactions on Instrumentation and Measurement*, vol. 67, no. 9, pp. 2177–2187, 2018.

[11] P. Visalakshi and C. Aarthi, "Textile industry waste water monitoring system using lora technology," *Artificial Intelligence for Internet of Things*, vol. 12, no. 1, pp. 189–196, 2019.

[12] X. Zhang, M. Zhang, F. Meng, Y. Qiao, S. Xu, and S. Hour, "A low-power wide-area network information monitoring system by combining nb-iot and lora," *IEEE Internet of things Journal*, vol. 6, no. 1, pp. 590–598, 2018.

[13] B. Xie and J. Xiong, "Combating interference for long range lora sensing," in *Proceedings of ACM SenSys*, 2019.

[14] F. Zhang, Z. Chang, K. Niu, J. Xiong, B. Jin, Q. Lv, and D. Zhang, "Exploring lora for long-range through-wall sensing," in *Proceedings of UbiComp*, 2020.

[15] L. Chen, J. Xiong, X. Chen, S. I. Lee, K. Chen, D. Han, D. Fang, Z. Tang, and Z. Wang, "Widesee: Towards wide-area contactless wireless sensing," in *Proceedings of ACM SenSys*, 2019.

[16] X. Xia, Y. Zheng, and T. Gu, "Litenap: Downclocking lora reception," *IEEE/ACM Transactions on Networking*, vol. 29, no. 6, pp. 2632–2645, 2021.

[17] L. Liu, Y. Yao, Z. Cao, and M. Zhang, "Deeplora: Learning accurate path loss model for long distance links in lpwan," in *Proceedings of IEEE INFOCOM*, 2021.

[18] C. Li, H. Guo, S. Tong, X. Zeng, Z. Cao, M. Zhang, Q. Yan, L. Xiao, J. Wang, and Y. Liu, "Nelora: Towards ultra-low snr lora communication with neural-enhanced demodulation," in *Proceedings of SenSys*, 2021.

[19] W. Gao, W. Du, Z. Zhao, G. Min, and M. Singhal, "Towards energy-fairness in lora networks," in *Proceedings of ICDCS*, 2019.

[20] W. Gao, Z. Zhao, and G. Min, "Adaplora: Resource adaptation for maximizing network lifetime in lora networks," in *Proceedings of ICNP*, 2020.

[21] L. Alliance, "Coverage and operator maps." Available: https://lora-alliance.org/lorawan-coverage/.

[22] A. Gamage, J. C. Liando, C. Gu, R. Tan, and M. Li, "Lmac: Efficient carrier-sense multiple access for lora," in *Proceedings of ACM MobiCom*, 2020.

[23] W. L. W. Group, "Ieee standard for local and metropolitan area networks–part 15.4: Low-rate wireless personal area networks," *IEEE Std 802.11-2012 (Revision of IEEE Std 802.11-2007)*, March 2012.

[24] W. S. N. Group, "Ieee standard for local and metropolitan area networks–part 15.4: Low-rate wireless personal area networks," *IEEE Std 802.15.4g-2012 (Amendment to IEEE Std 802.15.4-2011)*, April 2012.

[25] Semtech, "Sx1261/2 long range, low power, sub-ghz rf transceiver," Available: https://www.semtech.com/products/wireless-rf/lora-core/sx1262.

[26] ——, "Sx1276/77/78/79 137 mhz to 1020 mhz low power long range transceiver. rev. 7." Available: https://www.semtech.com/products/wireless-rf/lora-core/sx1276.

[27] L. Alliance, "Lorawan regional parameters v1.1." Available: https://lora-alliance.org/resource_hub/lorawan-regional-parameters-v1-1ra/.

[28] Semtech, "Sx126x cad performance evaluation," Available: https://lora-developers.semtech.com/library/product-documents/.

[29] C. Pham, "Investigating and experimenting csma channel access mechanisms for lora iot networks," in *Proceedings of IEEE WCNC*, 2018.

[30] M. O'kennedy, T. Niesler, R. Wolhuter, and N. Mitton, "Practical evaluation of carrier sensing for a lora wildlife monitoring network," in *Proceedings of IEEE IFIP*, 2020.

[31] S. Ahsan, S. A. Hassan, A. Adeel, and H. K. Qureshi, "Improving channel utilization of lorawan by using novel channel access mechanism," in *Proceedings of IEEE IWCMC*, 2019.

[32] C. Pham and M. Ehsan, "Dense deployment of lora networks: Expectations and limits of channel activity detection and capture effect for radio channel access," *Sensors*, vol. 21, no. 3, pp. 825–846, 2021.

[33] S. Tong, Z. Shen, Y. Liu, and J. Wang, "Combating link dynamics for reliable lora connection in urban settings," in *Proceedings of MobiCom*, 2021.

[34] J. Chan, A. Wang, A. Krishnamurthy, and S. Gollakota, "Deepsense: Enabling carrier sense in low-power wide area networks using deep learning," *arXiv preprint arXiv:1904.10607*, 2019.

[35] J. Jiang, Z. Xu, F. Dang, and J. Wang, "Long-range ambient lora backscatter with parallel decoding," in *Proceedings of MobiCom*, 2021.

[36] X. Xia, Y. Zheng, and T. Gu, "Ftrack: Parallel decoding for lora transmissions," *IEEE/ACM Transactions on Networking*, vol. 28, no. 6, pp. 2573–2586, 2020.

[37] X. Xia, N. Hou, Y. Zheng, and T. Gu, "Pcube: scaling lora concurrent transmissions with reception diversities," in *Proceedings of MobiCom*, 2021.

[38] S. Tong, J. Wang, and Y. Liu, "Combating packet collisions using non-stationary signal scaling in lpwans," in *Proceedings of MobiSys*, 2020.

[39] Z. Xu, P. Xie, and J. Wang, "Pyramid: Real-time lora collision decoding with peak tracking," in *Proceedings of INFOCOM*, 2021.

[40] K. N. Choi, H. Kolamunna, A. Uyanwatta, K. Thilakarathna, S. Seneviratne, R. Holz, M. Hassan, and A. Y. Zomaya, "Loradar: Lora sensor network monitoring through passive packet sniffing," *ACM SIGCOMM Computer Communication Review*, vol. 50, no. 4, pp. 10–24, 2020.

[41] A. F. Bravo-Montoya, J. S. Rondón-Sanabria, and E. E. Gaona-Garcí, "Development and testing of a real-time lorawan sniffer based on gnuradio," *TecnoLógicas*, vol. 22, no. 46, pp. 130–139, 2019.